End effects in linear tubular motors and compensated position sensorless control based on pulsating voltage injection

Francesco Cupertino, *Member, IEEE*, Paolo Giangrande, *Student Member, IEEE*,
Gianmario Pellegrino, *Member, IEEE*, and Luigi Salvatore

***Abstract*- The sensorless position control of permanent magnet synchronous motors can be successfully implemented by superimposing a high-frequency voltage signal on the control voltage. In this paper the position estimation is obtained by means of a high-frequency sinusoidal voltage signal injected along the estimated d-axis. Several methods proposed in the literature obtain the position estimation by tracking the zero condition of the high-frequency q current component. We propose a new approach that also exploits the d-axis high-frequency current component, allows working with injected voltage signal of reduced amplitude thus reducing noise and additional losses. The main contribution of paper relies in the compensation of the motor end-effects, due to the finite length of the tubular motor armature. These effects must be taken into account in the motor modeling because cause an error in the position estimation that is variable with the motor position. The modeling of the phenomenon and a proper compensation technique are proposed in the paper. Last, a simplified I-type controller is used to estimate motor position instead of the commonly adopted PI controller plus integrator and this requires a low-effort design. Experiments on a linear tubular permanent-magnet synchronous motor prototype are presented to validate the theoretical analysis and evidence the feasibility of the proposed sensorless technique.**

I. INTRODUCTION

Linear permanent magnet synchronous motors (LPMSMs) are becoming increasingly widespread in automation applications because they permit to eliminate mechanical transmission devices. Among the commonly used structures for LPMSMs the tubular one allows to better exploit the permanent magnet flux reducing size and end effects. Similarly to synchronous rotating machines the LPMSMs need position information to synchronize the current vector phase angle to the permanent magnets position. Since low and zero speed operations are essential in most practical applications, signal injection-based schemes appear a necessary solution for sensorless operation. As a matter of fact, at low and zero speed the back EMF voltage magnitude is very small or zero and this makes all the techniques based on the back EMF unsuccessful [1-2]. Recently, a large effort has been dedicated to investigate techniques for position estimation of synchronous motors using the injection of high-frequency signals [2-11] or using PWM excitation [12-13]. A high-frequency voltage signal can be superimposed on the motor control voltages to estimate the rod position from the resulting high-frequency current components that are affected by the motor magnetic saliency. This allows realizing sensorless schemes that don't require additional hardware, are not sensitive to parameter variations and have been proven to be successful at low and zero speed regardless the loading condition. The high-frequency injected voltage signal can be a rotating voltage vector in the stationary frame [2-6] or a pulsating voltage vector in the estimated rotor frame [5-10].

In this paper we consider the approach based on the superimposition of a pulsating voltage vector (PVV) along the estimated d-axis at a constant frequency. This approach has a low sensitivity to the inverter non-idealities [7] and is almost acoustically noiseless because the amount of high-frequency current injected into the q-axis is very small and this reduces the torque pulsations with respect to rotating injection methods [7-8]. The position estimation can be based on the analysis of the phase or amplitude of the negative and positive sequence currents at injection frequency [5] or on the minimization of the q-axis high-frequency current by means of a position observer [8,10]. The latter approach requires a lower computational effort because avoids multiple coordinate transformations but has a reduced sensitivity due to the low value of the high-frequency q-axis current component.

In this paper we propose an improved position observer that exploits the information contained in both d- and q-axis high-frequency currents. Moreover, as major original contribution of this paper with respect to [9], a novel compensation method is proposed for taking into account the motor end-effects, that would lead the standard tracking methods to instability. The finite length of the motor armature makes the high-frequency magnetic model of the motor variable with the position, thus introducing an estimation error that is also variable with the motor position. For this reason a compensated reference frame is introduced besides the estimated dq reference frame. Finally, a simple I type controller is used for the position observer instead of the common PI controller plus integrator. This simplifies the tuning procedure for the position estimation scheme. Experimental results obtained using a LPMSM prototype are shown in this paper to demonstrate the feasibility of the proposed position estimation scheme.

II. LINEAR TUBULAR PERMANENT MAGNET SYNCHRONOUS MOTORS

Linear electrical machines allow to directly generate force to the payload and find application in several fields ranging from transportation to industrial automation and power generation. In this work we consider three-phase linear actuators of the tubular topology. Due to the finite length of the machine two of the three armature phases have one end coil at the two opposite motor end, while the third phase does not. This implies that the mutual coupling between the three phases is not the same, and in particular it is lower for those two phases with one end coil. This effect can be observed in general in any kind of linear machine and will be hereinafter referred as end-effect of the

linear machine. To focus such effect Figure 1 reports the results of a FEM (Finite Element Method) simulation of a simplified tubular motor armature having only three coils, one for each phase. There is no PM contribution in the simplified model. Two simulations were carried out supplying only phase C and only phase A respectively. Figure 1 reports the field distribution in the two cases. From figure 1a it is evident that the mutual inductances M_{BC} and M_{CA} are equal, while from figure 1b results that the mutual inductance M_{AB} has a lower value with respect to M_{AC}. (=M_{CA}.). Practical windings adopt a number of coils multiple of three (for symmetry reasons). The asymmetry of the mutual inductances decreases with the number of coils and also with slotted armature but is always present in linear machines.

The linear tubular permanent magnet machine is constituted by an armature containing the three-phase windings and a rod containing the permanent magnets [19]. The rod can be internal or external with respect to the armature and both topologies could be either moving rod or moving armature. The armature can be air-cored or iron-cored and in the latter case it could be slotted or slotless. Armature teeth increase the average force at the expenses of an increased cogging force. The topology considered in this work has an inner rod and a moving armature, iron cored and slotless. This is a typical solution for applications in tool machines (pick and place, XY machines). The magnets inside the rod could have axial or radial magnetization [20]. In the first case the motor presents saliency and is usually referred as internal permanent magnet (IPM). In the latter case the motor is referred as surface permanent magnet (SPM). The first configuration is better suited for the implementation of the sensorless control based on signal injection because this control technique exploits the motor saliencies for the estimation of the motor position.

A qualitative section of the IPM tubular motor used in this work is presented in figure 2. The magnets are separated by iron pole pieces and the different permeability of iron and permanent magnets produces the saliency of the motor: all the inductances (phase self-inductances and mutual inductances) are functions of the motor position because the magnetic coupling is higher when the field path includes the rod iron while it is lower when it does not. Figure 3 reports a portion of the section of the IPM motor showing the relative position of coils magnets and spacers. The α-axis coincides with the phase A axis and is used as reference for position measurement. The d-axis is defined as the direction of the equivalent north pole of the rod, that corresponds to the center of a spacer. When the d-axis is coincident with the α-axis the phase A self inductance is minimum because magnets are aligned with phase A coils (see figure 3a). In figure 3b the rod position is $-\pi/6$. In such position the mutual inductance between phase A and phase B is minimum because magnets are aligned with the center of (+B) and (-A) coils (as well as (-B) and (+A)). The same mutual inductance has its maximum value when the rod position is $\pi/3$ (see figure 3c) because the iron spacers take the place of the magnets.

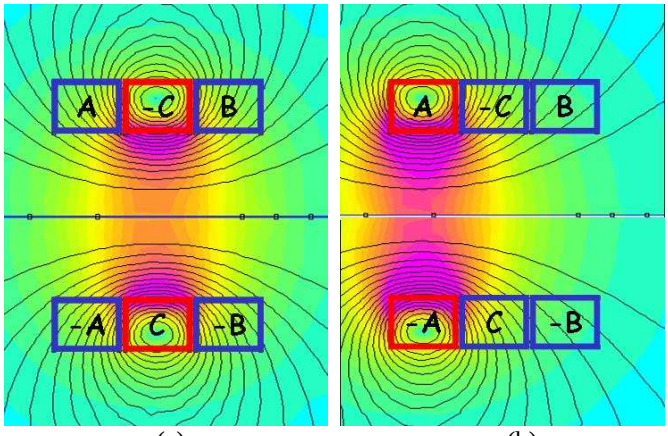

(a) (b)

Figure 1 – Flux distribution obtained when only phase C (left figure) or only phase A (right figure) is supplied.

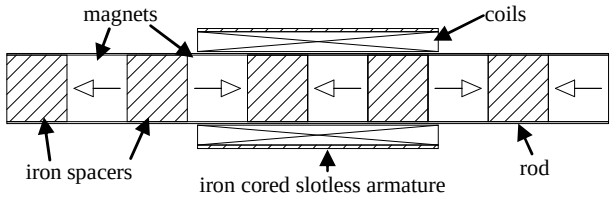

Figure 2 - Qualitative section of the IPM tubular linear motor used in this work.

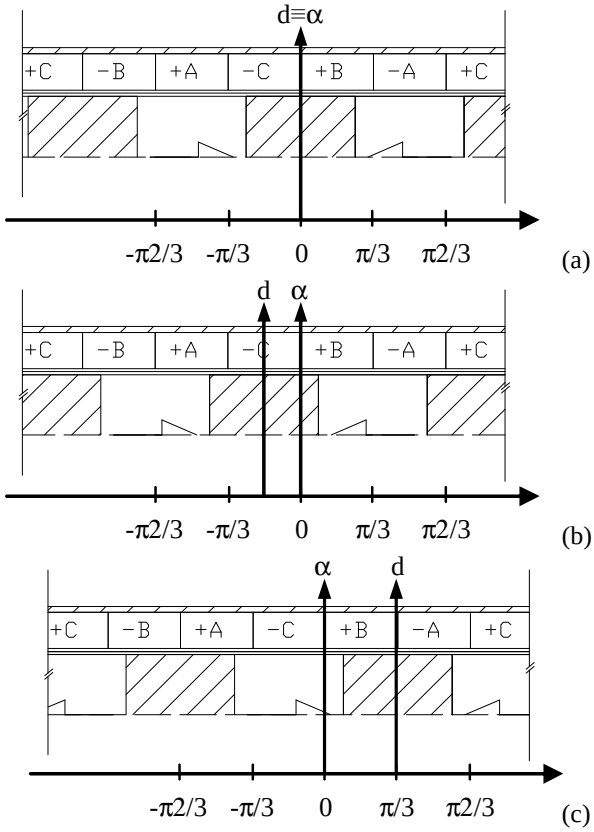

Figure 3 - Section of the IPM tubular linear motor showing the relative position of rod and armature: 0 (a), $-\pi/6$ (b) and $\pi/3$ (c) electrical radians.

III. MEASURE OF THE MOTOR INDUCTANCES

The motor self and mutual phase inductances at injection frequency have been measured by means of a dedicated test bench. Each phase, in turn, was supplied with a 1000 Hz voltage with constant amplitude using a Chroma 61703 power supply. The current of the supplied motor phase and the voltages of the two non supplied phases were measured at different positions of the motor rod using oscilloscope probes (see figure 4). The test was repeated three times for evaluating the self and mutual inductances of all the motor phases. The measured inductances are reported in figure 5a as function of motor position and expressed in both the ABC and the dq reference frame. The results show that the inductances are function of the motor position and their shape agrees with the considerations reported in the previous section. The waveforms are not exactly sinusoidal due to the rod shape and in particular to the magnet length that is nearly twice the spacer length. With different lengths (e.g. magnet equal to spacer) more sinusoidal inductances would be achieved. Going back to figure 5a, phase A self inductance is minimum when position is zero and the mutual term $|M_{AB}|$ is minimum at $-\pi/6$ and maximum at $\pi/3$ (all the mutual inductances are negative due to the adopted convention). Moreover the A-B mutual term M_{AB} has a lower average value than the other two mutual terms due to the end effect. The obtained results permit to approximate the mutual terms according to (1) where M_0 is the average value of the M_{AB} term, ΔM_0 is the difference between the average mutual terms and M_2 is the amplitude of the mutual inductance oscillation:

$$\begin{cases} M_{AB} = M_0 + M_2 \cos\left(2\theta - \frac{2}{3}\pi\right) \\ M_{BC} = M_0 + M_2 \cos(2\theta) + \Delta M_0 \\ M_{CA} = M_0 + M_2 \cos\left(2\theta + \frac{2}{3}\pi\right) + \Delta M_0 \end{cases} \quad (1)$$

The contribution of the ΔM_0 term to the motor flux is given by (2) using phase coordinates:

$$\Delta\boldsymbol{\lambda}_{ABC} = \begin{bmatrix} 0 & 0 & \Delta M_0 \\ 0 & 0 & \Delta M_0 \\ \Delta M_0 & \Delta M_0 & 0 \end{bmatrix} \mathbf{i}_{ABC} \quad (2)$$

After some manipulations, equation 2 can be expressed in the dq reference frame:

$$\Delta\boldsymbol{\lambda}_{dq} = -\frac{2}{3}\Delta M_0 \begin{bmatrix} 1+\cos\left(2\theta-\frac{2}{3}\pi\right) & -\sin\left(2\theta-\frac{2}{3}\pi\right) \\ -\sin\left(2\theta-\frac{2}{3}\pi\right) & 1-\cos\left(2\theta-\frac{2}{3}\pi\right) \end{bmatrix} \mathbf{i}_{dq} \quad (3)$$

Equation 3 demonstrates that the end-effect term ΔM_0 produces a cross-coupling term L_{dq} and also a variable contribution to the L_d and L_q terms as also evidenced in figure 1b.

IV. HIGH FREQUENCY MODEL OF THE LPMSM

The high-frequency model of the motor can be derived in the hypothesis that the injection frequency is much higher than the motor speed, the back-EMF has no components at injection frequency, and the resistive drops are neglected [3,5]:

$$\begin{bmatrix} \lambda_d \\ \lambda_q \end{bmatrix} = \begin{bmatrix} L_d(\theta) & L_{dq}(\theta) \\ L_{dq}(\theta) & L_q(\theta) \end{bmatrix} \begin{bmatrix} i_d \\ i_q \end{bmatrix} \quad (4)$$

Since a high-frequency voltage (flux) vector is superimposed to the motor control voltages, the inverse relationship of (4) has to be derived.

By using the complex notation [14] and introducing the complex-conjugate flux $\boldsymbol{\lambda}^*_{dq} = \lambda_d - j\lambda_q$, equation (4) can be

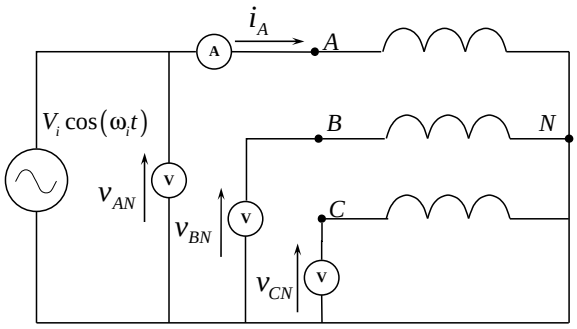

Figure 4 – Scheme used to measure the high frequency inductances

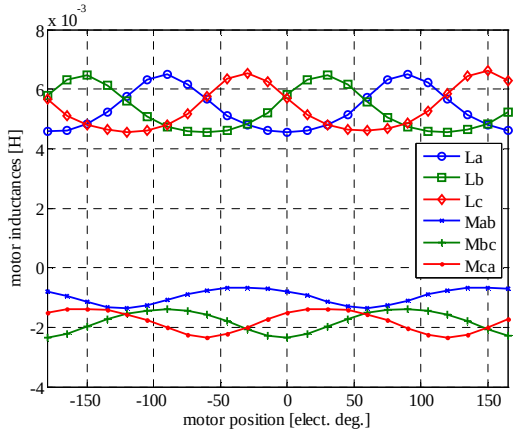

(a)

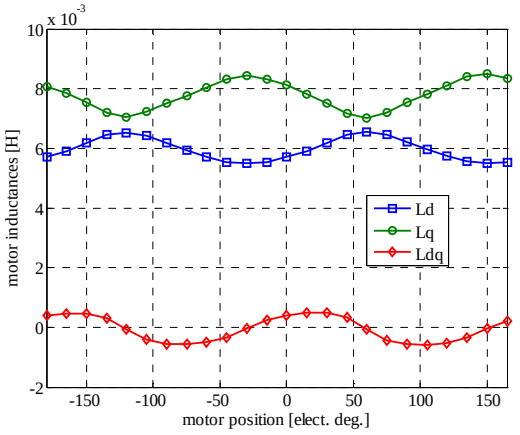

(b)

Figure 5 – Measured motor inductances at 1000 Hz in the abc (a) and dq (b) reference frame.

rewritten as (5) where positive and negative sequence components are evidenced:

$$\mathbf{i}_{dq} = \left(\frac{L_d(\theta) + L_q(\theta)}{2\Delta} \right) \boldsymbol{\lambda}_{dq} - \left(\frac{L_d(\theta) - L_q(\theta)}{2\Delta} + j \frac{L_{dq}(\theta)}{\Delta} \right) \boldsymbol{\lambda}^*_{dq} \quad (5)$$

where $\Delta = L_d(\theta) L_q(\theta) - L^2_{dq}(\theta)$. In the following the dependence of all the inductances from the motor position θ will be implied for simplicity. Equation (5) can be rewritten using the estimated dq reference frame, that leads the actual dq frame by θ_{err} radians $\left(\mathbf{x}_{dq} = \mathbf{x}^{est}_{dq} e^{j\theta err}, \theta^{est} = \theta + \theta_{err} \right)$ as defined in figure 6:

$$\mathbf{i}^{est}_{dq} = \left(\frac{L_d + L_q}{2\Delta} \right) \boldsymbol{\lambda}^{est}_{dq} - \left(\frac{L_d - L_q}{2\Delta} + j \frac{L_{dq}}{\Delta} \right) \boldsymbol{\lambda}^{est*}_{dq} e^{-j2\theta err} \quad (6)$$

In the proposed sensorless scheme a pulsating high frequency voltage signal is injected along the estimated d-axis, thus the high-frequency voltage (flux) along the estimated q-axis is zero. Equation (6) can be rewritten under the assumption $\boldsymbol{\lambda}^{est}_{dq} = \boldsymbol{\lambda}^{est*}_{dq} = \lambda^{est}_d$:

$$\mathbf{i}^{est}_{dq} = \left[\left(\frac{L_d + L_q}{2\Delta} - \frac{L_d - L_q}{2\Delta} \cos(2\theta_{err}) - \frac{L_{dq}}{\Delta} \sin(2\theta_{err}) \right) + j \left(\frac{L_d - L_q}{2\Delta} \sin(2\theta_{err}) - \frac{L_{dq}}{\Delta} \cos(2\theta_{err}) \right) \right] \lambda^{est}_d = \mathbf{R} \lambda^{est}_d \quad (7)$$

where $\boldsymbol{R}$ is a complex operator whose argument ψ is expressed in (8).

$$\psi = \arctan \left[\frac{(L_d - L_q)\sin(2\theta_{err}) - 2L_{dq}\cos(2\theta_{err})}{(L_d + L_q) - (L_d - L_q)\cos(2\theta_{err}) - 2L_{dq}\sin(2\theta_{err})} \right] \quad (8)$$

The angle ψ is the phase angle of the obtained high-frequency current with respect to the injected flux vector. It must be noticed that ψ is function both of the position estimation error and the motor electrical position by means of the L_d, L_q and L_{dq} terms. Figure 7a reports the angle ψ as function of the motor position for different values of the estimation error θ_{err}.

For a given estimation error θ_{err}, the argument ψ varies with respect to the motor position and in particular the sign of ψ changes at different rotor positions. As already said, the dependence on θ is due to the end-effects of the tubular motor. The red dashed curve in figure 7a demonstrates that with no estimation error the high-frequency current is still not aligned with estimated d-axis. In other words, having zero-current along the estimated q-axis does not mean that the motor position is estimated correctly, as it usually happens with rotating machines. A proper compensation method is then necessary. When the estimation error is zero the phase between flux and current becomes

$$\psi_{LUT} = \arctan \left[\frac{-L_{dq}}{L_q} \right] \quad (9)$$

The angle ψ_{LUT} is the red dashed line plotted in figure 7a. It is convenient to represent the high-frequency current in a compensated dq reference frame that is shifted from the estimated dq reference frame by ψ_{LUT} radians as also defined in figure 6.

Considering $\mathbf{x}^{comp}_{dq} = \mathbf{x}^{est}_{dq} e^{-j\psi_{LUT}}$, *and* $\theta^{comp} = \theta^{est} + \psi_{LUT}$ gives:

$$\mathbf{i}^{comp}_{dq} = \mathbf{i}^{est}_{dq} e^{-j\psi_{LUT}} = |\mathbf{R}| \lambda^{est}_d e^{j(\psi - \psi_{LUT})} \quad (10)$$

The argument ψ-ψ_{LUT}, evidenced in (10), is reported in figure 7b for the same values of θ_{err} considered in figure 7a. In the compensated reference frame the sign of phase-angle of the high-frequency current does not depend on motor position anymore.

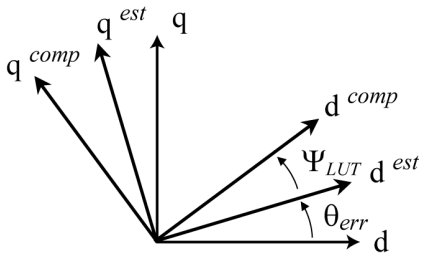

Figure 6 – Definition of the various reference frames needed for sensorless control: motor dq axes, estimated axes (d^{est}-q^{est}), compensated axes (d^{comp}-q^{comp}).

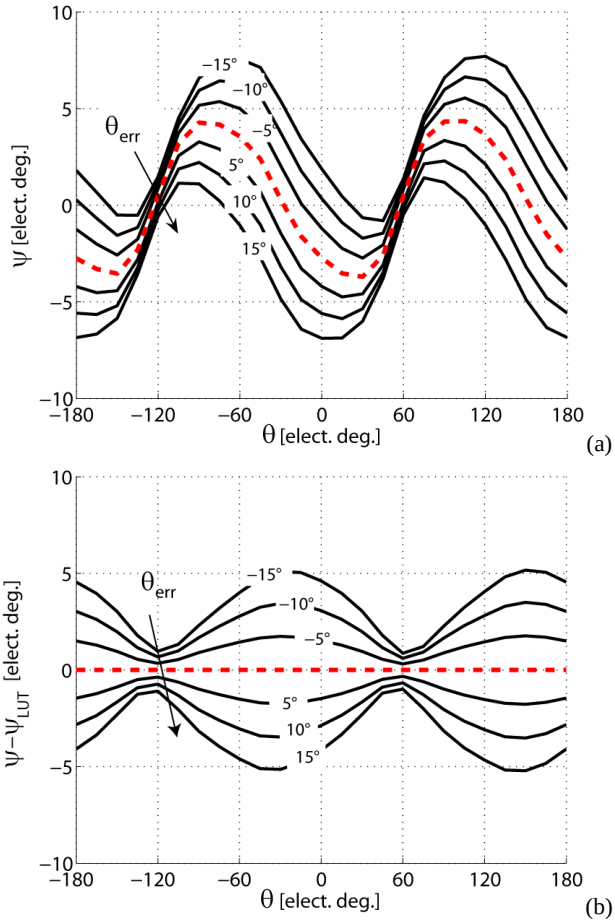

Figure 7 – Phase angle of the high-frequency current in the estimated (a) and in the compensated (b) dq reference frames for several values of the position estimation error between -15 and +15 electrical degrees.

In particular, when the high-frequency q-axis current in the compensated frame is zero, also the position error is zero and vice versa.

With pulsating voltage injection along the estimated d axis ($v_i = V_i \sin(\omega_i t + \pi)$), the injected flux is the one defined in (11):

$$\lambda_d^{est}(t) = \frac{V_i}{\omega_i}\cos(\omega_i t) \tag{11}$$

where V_i and ω_i are magnitude and pulsation of the injected voltage respectively. The product of the current components in the compensated reference frame can be easily derived using (10) and (11) and applying Werner formula:

$$i_d^{comp} i_q^{comp} = \frac{|R|^2 |V_i|^2}{2\omega_i^2}\left[1-\sin^2(\omega_i t)\right]\sin\left(2\left(\psi - \psi_{LUT}\right)\right) \tag{12}$$

A low pass filter can be used to remove the component at ω_i from (12):

$$LPF\left\{i_d^{comp} i_q^{comp}\right\} = \frac{|R|^2 |V_i|^2}{4\omega_i^2}\sin\left(2\left(\psi - \psi_{LUT}\right)\right) \tag{13}$$

As demonstrated in figure 7b, the angle ψ-ψ_{LUT} is zero only when the estimation error is zero, thus (13) is the error function that will be used here for tracking the rotor position by means of both a PI-type controller plus an integrator [7,10] and an I-type controller. It is important to underline once more that the high frequency voltage is injected along the estimated d-axis while the current demodulation must be performed in the compensated dq reference frame to take into account the end-effects of the tubular motor.

V. Sensorless Control Scheme

In most of the related literature the position estimation relies on the minimization of the low pass filtered product of the currents in the dq reference frame using different schemes. Usually a PI regulator gives the estimated speed and a successive integrator gives the estimated motor position [10, 15]. The modified approach here introduced estimates the position by minimizing the product given in (13) divided by the RMS value of i_d^{comp} (see figure 8). The RMS value is calculated using the last 16 samples, that correspond to one period of the 1 kHz injected voltage. Since $L_q > L_d$ in the considered prototype, i_d^{comp} reaches its largest amplitude when the estimation error is zero and decreases when the estimation error increases but always remains well above zero. Dividing by the RMS value of i_d^{comp} permits to increase the gain of the estimation loop when the estimation error increases thus improving the observer performances during transients. The experimental results showing the effect of the proposed division are reported in [9] and have been omitted for brevity.

An I-type controller can be used to estimate the motor position in place of the PI controller followed by an integrator. This does not compromise the zero steady state error condition that is guaranteed by a single integrator in the estimation loop [21]. In this way the scheme is simplified because, as it will be shown later, the selection of the single integral gain is straightforward, and can be performed off line. Moreover, removing an integrator from the open loop transfer function of the position observer gives a $\pi/2$ increase of the phase thus improving the stability margin.

In both the schemes presented in figure 8, the output of the integrator is the estimated motor position that is used for the current vector control and for the injection of the high-frequency voltage signal (see figure 11). The look-up table LUT contains the values of the angle ψ_{LUT} (6), that are added to the estimated position to obtain the compensated dq reference frame position. The compensated position is only used inside the position observer shown in figure 8.

The LUT values can be obtained using equation (6) by means of the measured inductances (see figure 5b) or it can be also derived directly during the experiments. As a matter of fact the compensating LUT has been also obtained in position sensorless control, changing the compensation angle until the estimation error became negligible. The operation was repeated 56 times in different motor position covering 360 electrical degrees. The two LUTs are reported in figure 9 and agree quite well. They have a peak value of about 4 electrical degrees and do not depend on motor load.

VI. Experimental Setup and Algorithm Commissioning

All the experimental investigations presented in this paper were performed using a dSPACE 1103 microcontroller board. Figure 10 shows the experimental test bench. The inverter switching frequency and the sample frequency of the control algorithm were set equal to 16 kHz and the inverter dead time was equal to 0.8 μs. The injected voltage amplitude V_i was 12 V and its frequency f_i = 1000 Hz, the generated high-frequency current was equal to about 0.5 A. The LPMSM rated parameters are as follows: rated current 2 A, R_s=9 Ω, polar pitch 56 mm (corresponding to 2π electrical radians), force constant 20 N/A.

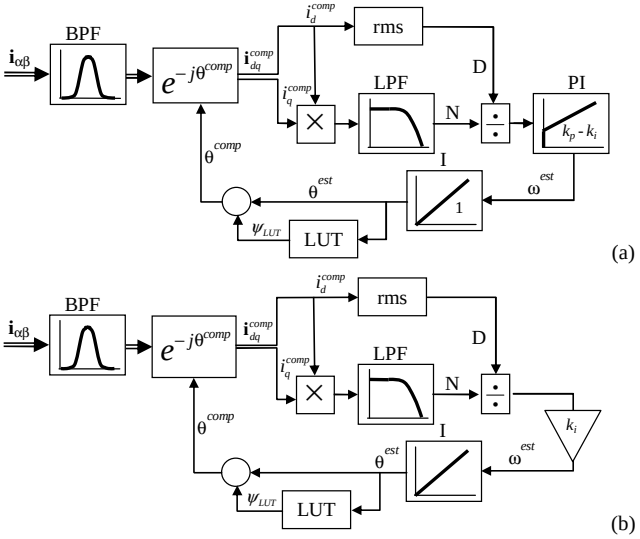

Figure 8. Signal flow graph of the improved position observer with PI regulator plus integrator (a) and a simplified version with an I-type regulator (b).

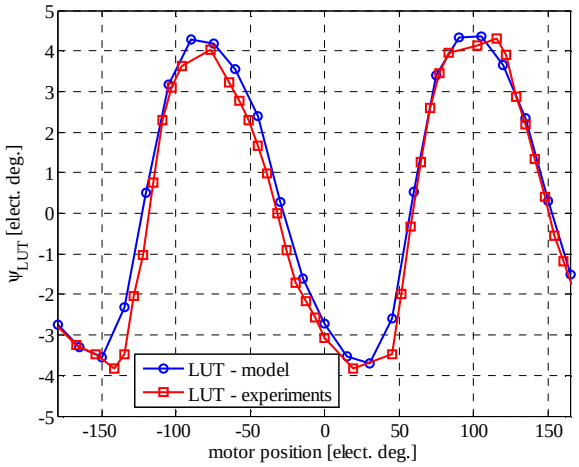

Figure 9. Compensating LUT obtained using the mathematical model (blue+circle) and directly measured under sensorless control (red+square).

Figure 10. LPMSM prototype used for the tests.

The motor inductances are the ones reported in figure 5. The DC bus voltage is 72 V. Figure 11 reports the block diagram of the vector control scheme. The stator resistance of the considered prototype is negligible in the high frequency impedance. Moreover R_s only affects the phase relation between voltages and currents in the time domain that is not utilized by the algorithm proposed for position estimation.

As shown in figure 8, the band-pass filters are implemented in the stationary reference frame because they compromise observer transient performances if executed after the coordinate transformation. In the stationary reference frame the injected components are at injection frequency plus the motor stator frequency $\omega_r/2\pi$. The band-pass filters are second-order Butterworth filters centered at f_i with 100 Hz bandwidth so to guarantee efficient signal processing in the motor low-speed range [16]. The first order LPF, that removes the $2\omega_i$ component and noise from the product (13) has 5 ms time constant that has been selected by trial and error.

The selection of PI or I controller gains in the position observer has been performed off-line, using a linear encoder to close the control loops and comparing the estimated and measured values. One of the contributions of this paper is the introduction of a simplified position observer that reduces instability problems and shortens the observer tuning. When the observer is running off-line it is simple to select an adequate value for the integral gain with a few tests. If the gain is too low the position estimate tracks the measured one with considerable delay, and evident estimate oscillations occur when the integral gain is too high. Figure 12 evidences the steps followed to tune the integral gain.

We did not experience observer instability with the I-type controller. On the contrary, a poor choice of the gains in the scheme with the PI controller plus integrator can lead to instability and a longer procedure is required to reach the same level of accuracy obtained with the simplified scheme. To obtain a fair comparison of the two observers shown in figure 8, the proportional gain of the PI controller was chosen equal to the gain of the integral one in the tests shown in the next section.

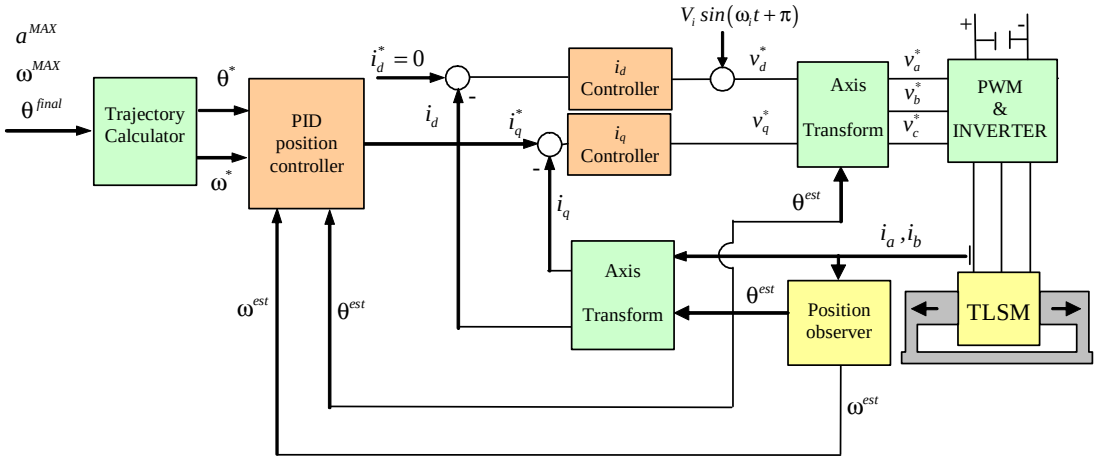

Figure 11. Block diagram of the drive.

VII. EXPERIMENTAL RESULTS

The position reference used for the tests here presented was a minimum time trajectory for a 28 mm (π radians) movement [17]. For the tests presented here the maximum acceleration was set equal to 5 m/s^2. Figure 13 reports the position references and the position estimation errors obtained during some no-load tests and using trajectories with different peak speeds. The peak position error is below 12 electrical degrees when the maximum speed is limited to 50 mm/s and raises to 24 degree and 36 degree when the maximum speed is 200 mm/s and 300 mm/s respectively. The speed range could be extended by the adoption of a model based scheme as proposed in [18].

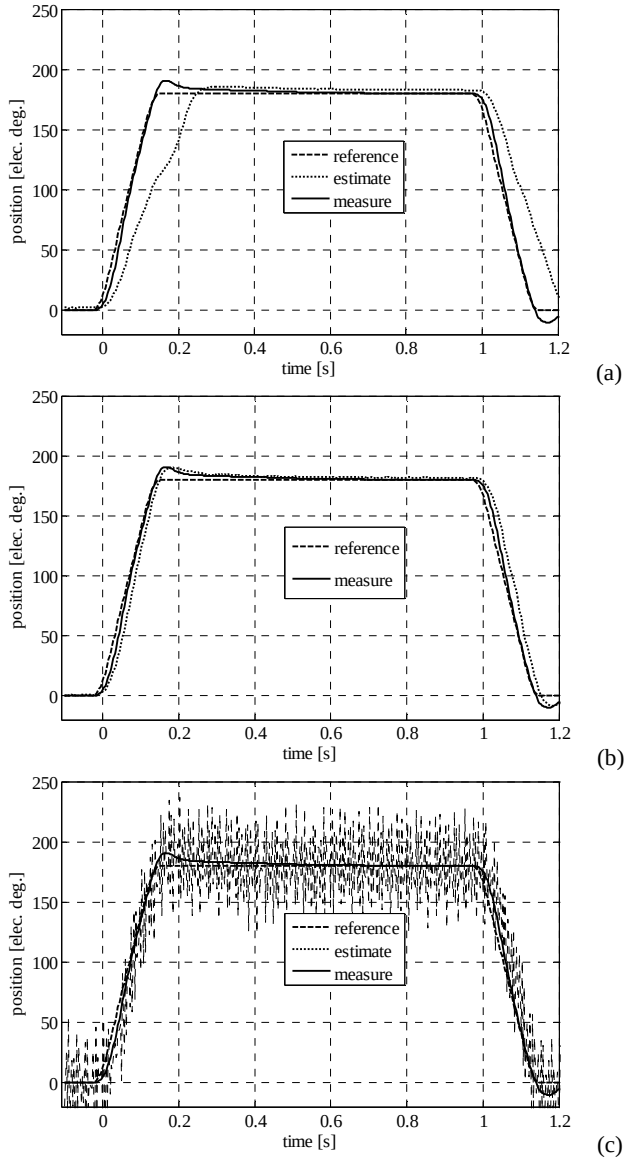

Figure 12. I controller tuning procedure results: measured and estimated position obtained using the observer in open loop and with an integral gain equal to 600 (a), 23000 (b), and 150000 (c).

Figure 14 reports the position, position errors and i_q current responses measured during a test in which a 20 N constant external force was applied to the motor and the maximum speed was set to 200 mm/s. During the loaded test a weight is connected to the motor mover using a metal cable and a pulley. In this way a constant force equal to 20 N was applied to the motor in the direction of the connected cable. This implies that the machine is working as a brake during the first movement and as a motor in the second movement shown in figure 14a.

Figure 14a compares the responses obtained under sensorless and sensored control using the same parameters for the cascaded position speed and current control loops. Performances are comparable, even if the position control bandwidth could be increased under sensored control but is limited to a few Hz in sensorless conditions.

The position performances are comparable but the estimation error is higher in motoring phase (about 33 electrical degrees peak error) as the figure 14b shows. The steady state position estimation error is always below 1 electrical degree (150 µm for the considered prototype) at steady state. Figure 14b reports two curves of position errors obtained with the different position observers shown in figure 8. It is evident that the performances of both schemes are comparable. Figure 14b demonstrates that the use of a single I controller does not reduce estimation accuracy during transients but simplifies the control scheme commissioning.

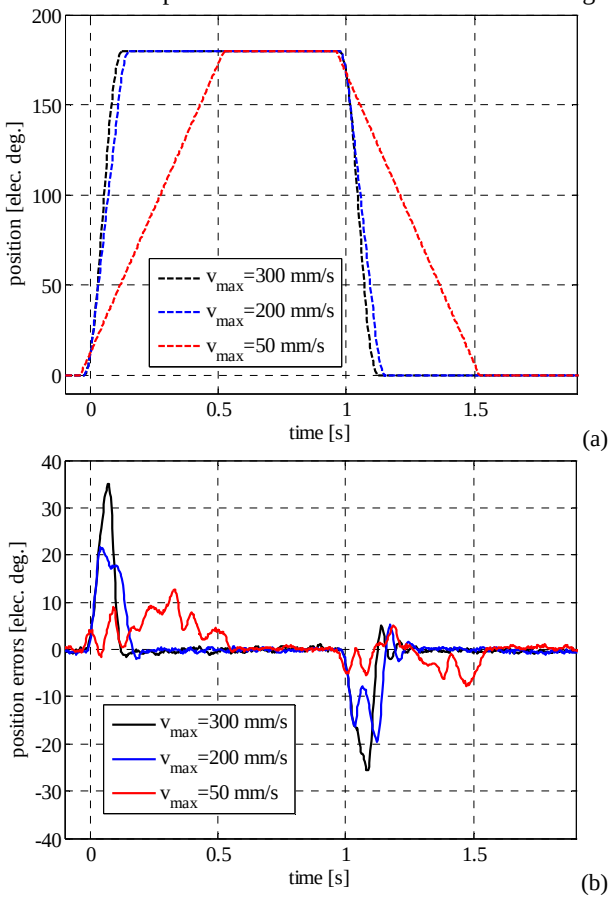

Figure 13. Position reference trajectories (a) and estimation error (b) under sensorless position control at different peak speeds (no-load).

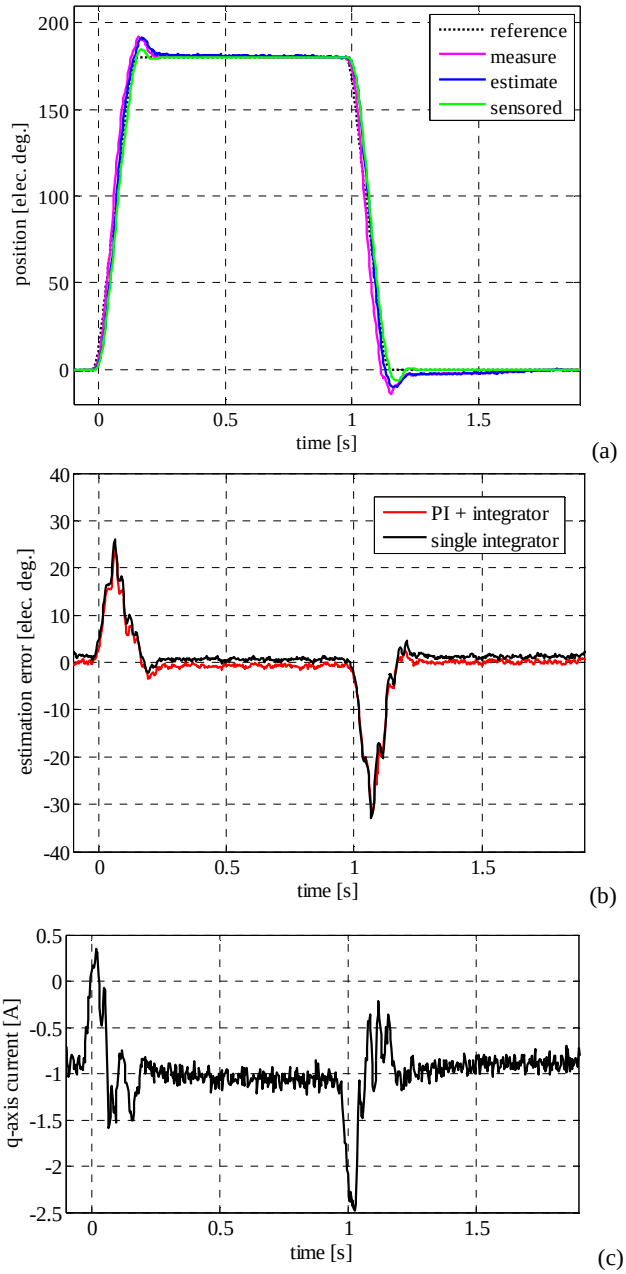

Figure 14. Comparison of the performances obtained using the PI + integrator controller and the proposed single I controller: position trajectory (a), estimation errors under 20N load force (b) and i_q response (c).

VIII. CONCLUSIVE REMARKS

In this paper, an improved sensorless control algorithm for LPMSMs based on high-frequency pulsating voltage injection has been presented. The method is suitable for machines with reduced saliency and utilizes a simple I controller rather than a PI controller plus integrator in the position observer. The error due to motor end-effects has been evidenced, modeled and compensated by means of a new reference frame adopted for high-frequency current demodulation. The position of the compensated reference frame is stored in a LUT that can be obtained either by measuring the motor inductances or directly by experiments. The algorithm exploits the information contained in both the d-q axes current components. This guarantees a better signal-to-noise ratio to the signal processing technique and permits to reduce the amplitude of the injected voltage.

All considered, the estimation scheme is as simple as possible for a motor with such little saliency and position-dependent non-idealities. The design criteria given in the paper make straightforward the commissioning procedure and avoid the risk of instability. Moreover the estimation accuracy of the proposed observer is almost not affected by the load current value.

REFERENCES

[1] J. Holtz, "Sensorless Control of Induction Machines—With or Without Signal Injection?", IEEE Transactions on Industrial Electronics, Volume 53, Issue 1, Feb. 2006, pp. 7 – 30.

[2] C. Silva, G.M. Asher and M. Sumner, "Hybrid rotor position observer for wide speed ranger Sensorless PM motor drives including zero speed", IEEE Transactions on Industry Electronics, Vol. 53, N° 2, April 2006.

[3] C. Silva, G.M. Asher, and M. Sumner, "Influence of dead-time compensation on rotor position estimation in surface mounted PM machines using HF voltage injection," in Proc. IEE-J/IAS PCC, Osaka, Japan, Apr. 2002, pp. 1279 – 1284.

[4] C. Silva, G.M. Asher and M. Sumner, "Sensorless rotor position control in a surface mounted PM machine using HF voltage injection" Proceedings of IEEE Power Electronics and Motion Control Conference, Dubrovnik, 2002.

[5] H. Kim and R.D. Lorenz, "Carrier signal injection based sensorless control methods for IPM synchronous machine drives", Conference Record of the 2004 IEEE Industry Applications Conference, 2004. 39th IAS Annual Meeting. Vol. 2, 3-7 Oct. 2004 Page(s):977 – 984.

[6] N. Bianchi, and S. Bolognini, "Influence of rotor geometry of an IPM motor on sensorless control feasibility", IEEE Transactions on Industry Applications, Vol. 43, N° 1, January-February 2007, pp. 87 – 96.

[7] M. Linke, R. Kennel and J. Holtz, "Sensorless speed and position control of synchronous machines using altarnating carrier injection", proceedings of IEMDC, IEEE Electric Machines and Drivers Conference, Madison, WI, Jun. 2–4, 2003, pp. 1211 – 1217.

[8] J.H. Jang, J.I. Ha, M. Ohto, K. Ide and S.K. Sul, "Analysis of permanent magnet machine for sensorless control based on high frequency signal injection", IEEE Transactions on Industry Applications, Vol. 40, N° 6, Nov/Dec 2004.

[9] F. Cupertino, P. Giangrande, L. Salvatore, G. Pellegrino: "Sensorless position control of linear tubular motors with pulsating voltage injection and improved position observer", Proc of IEMDC 09, IEEE International Electrical Machines and Drives Conference, Miami, USA, 3-6 May 2009.

[10] J. Holtz, "Acquisition of Position Error and Magnet Polarity for Sensorless Control of PM Synchronous Machines", IEEE Transactions on Industry Applications, Vol. 44, n. 4, July-Aug. 2008 Page(s):1172 – 1180.

[11] A. Consoli, G. Scarcella and A. Testa, "Sensorless control of PM synchronous motors at zero speed", Proc. IEEE IAS Annual Meeting, Phoenix, Arizona, Oct. 1999, pp. 1033 – 1040.

[12] Qiang Gao, Greg M. Asher, Mark Sumner, and Lee Empringham, "Position Estimation of a Matrix-Converter-Fed AC PM Machine From Zero to High Speed Using PWM Excitation", IEEE Transactions on Industrial Electronics, vol. 56, no. 6, June 2009, pp. 2030-2038.

[13] Ji-Liang Shi, Tian-Hua Liu, and Yung-Chi Chang, "Position Control of an Interior Permanent-Magnet Synchronous Motor Without Using a Shaft Position Sensor" IEEE Transactions on Industrial Electronics, vol. 54, no. 4, August 2007, pp. 1989-1999.

[14] P. Guglielmi, M. Pastorelli and A. Vagati, "Cross saturation effects in IPM motors and related impact on zero-speed sensorless control", IEEE Trans. on Industry Applications, Vol. 42, Issue 6, Nov-Dec. 2006 Page(s):1516 – 1522.

[15] D. Raca, P. Garcia, D. Reigosa, F. Briz and R.D. Lorenz, "Carrier Signal Selection for Sensorless Control of PM Synchronous Machines at Zero and Very Low Speeds", Proc. IEEE IAS Annual Meeting, Phoenix, Arizona, 5-9 Oct. 2008, Edmonton, Canada.
[16] J.G. Proakis and D.G. Manolakis, Digital signal processing, 3rd ed., Prentice Hall, 1996.
[17] G. Lo Bianco R. Zanasi, A. Tonielli, Nonlinear filters for the generation of smooth trajectories, Automatica, Vol. 36, 2000, pp. 439 – 448.
[18] Antti Piippo, Marko Hinkkanen, and Jorma Luomi, "Analysis of an Adaptive Observer for Sensorless Control of Interior Permanent Magnet Synchronous Motors", IEEE Transactions on Industrial Electronics, vol. 55, no. 2, February 2008, pp. 570-576
[19] Jiabin Wang, Geraint W. Jewell, and David Howe, "A General Framework for the Analysis and Design of Tubular Linear Permanent Magnet Machines", IEEE Transactions on Magnetics, vol. 35, no. 3, May 1999, pp. 1986-2000.
[20] N. Bianchi, S. Bolognani, D. Dalla Corte, and F. Tonel, "Tubular linear permanent magnet motors: an overall comparison", IEEE Transactions on Industry Applications, vol. 39, no. 2, March/April 2003, pp. 466-475.
[21] F. Cupertino, P. Giangrande, "A simplified position observer for zero-speed sensorless control of synchronous motors", Proc. of IECON 09 The 35th Annual Conference of the IEEE Industrial Electronics Society, Porto, Portugal, November 3-5, 2009.